Received: 29 June 2020 | Revised: 29 October 2020 | Accepted: 15 December 2020

DOI: 10.1002/aic.17152

SEPARATIONS: MATERIALS, DEVICES AND PROCESSES

AIChE JOURNAL

A stable metal–organic framework with well-matched pore cavity for efficient acetylene separation

Yang Chen[1] | Yadan Du[1] | Yong Wang[1] | Rajamani Krishna[2] | Libo Li[1,3] | Jiangfeng Yang[1,3] | Jinping Li[1,3] | Bin Mu[4]

[1]College of Chemistry and Chemical Engineering, Shanxi Key Laboratory of Gas Energy Efficient and Clean Utilization, Taiyuan University of Technology, Taiyuan, China

[2]Van't Hoff Institute for Molecular Sciences, University of Amsterdam, Amsterdam, The Netherlands

[3]Key Laboratory of Coal Science and Technology, Ministry of Education and Shanxi Province, Taiyuan University of Technology, Taiyuan, China

[4]Chemical Engineering, School for Engineering of Matter, Transport, and Energy, Arizona State University, Tempe, Arizona

Correspondence
Libo Li, College of Chemistry and Chemical Engineering, Shanxi Key Laboratory of Gas Energy Efficient and Clean Utilization, Taiyuan University of Technology, Taiyuan 030024, Shanxi, China.
Email: lilibo908@hotmail.com

Bin Mu, Chemical Engineering, School for Engineering of Matter, Transport, and Energy, Arizona State University, Tempe, AZ 85287.
Email: bmu@asu.edu

Funding information
National Natural Science Foundation of China, Grant/Award Numbers: 21908155, 21922810, 21878205; Natural Science Foundation for Young Scientists of Shanxi Province, Grant/Award Number: 201901D211053

Abstract

Acetylene, an important petrochemical feedstock, is the starting chemical to produce many polymer products. Separating C_2H_2 from its by-product mixtures is still an energy-consuming process and remains challenging. Here, we present a metal–organic framework[Zn_2(bpy)(btec)], with a desirable pore geometry and stable framework, which demonstrated a high separation performance of C_2H_2 from simulated mixtures. With the desirable pore dimension and hydrogen bonding sites, Zn_2(bpy)(btec) shows by far the both highest C_2H_2/C_2H_4 and C_2H_2/CO_2 uptake ratios, very high adsorption selectivities and moderately C_2H_2 uptake of 93.5 cm^3/cm^3 under 298 K and 1 atm. Not only straightforwardly produced high purity of C_2H_4, but also recovered high purity of C_2H_2 (>98%) in the regeneration process (>92% recovery). More notably, Zn_2(bpy)(btec) can be straightforwardly synthesized at a large scale under environmentally friendly conditions, and its good water/chemical stability, thermostability, and cyclic stability highlight the promise of this molecular sieving material for industrial C_2H_2 separation.

KEYWORDS
ethylene purification, gas separation, MOFs, size sieving, structural stability

1 | INTRODUCTION

Both acetylene (C_2H_2) and ethylene (C_2H_4) are widely used as basic chemical materials in the petrochemical industry. The production of C_2H_4 is from the fractional distillation of petroleum, which usually coexists with 1% C_2H_2.[1-3] In addition, carbon dioxide (CO_2) appears in the production of C_2H_2 by the thermal cracking process.[4,5] Thus, selectively separation of C_2H_2 from C_2H_4/C_2H_2 or CO_2/C_2H_2 mixtures is important to meet the requirement of polymer-grade C_2H_4 and high-purity C_2H_2 in petrochemical industrials.[6,7] However, considering the small difference of molecular dimension of C_2H_2 (3.3 Å × 3.3 Å × 5.7 Å), C_2H_4 (3.3 Å × 4.2 Å × 4.8 Å) and CO_2 (3.2 Å × 3.3 Å × 5.4 Å), as well as their similar physical properties, it is a very challenging to separate C_2H_2 from C_2H_4 or CO_2.[8,9] Although the cryogenic distillation for C_2H_2 separation is a very mature operation, it requires huge capital and energy input primarily due to the requirement of low temperature operation.[10-12] It is necessary to develop a more efficient separation process such as porous materials based adsorptive separation with relatively low energy consumption and favorable regeneration.[13,14]

Porous materials, such as zeolites, metal–organic frameworks (MOFs) and covalent-organic frameworks (COFs), with porous

structures, huge specific surface area, and designable frameworks have received extensive attention in recent years,[15-17] as they present great potential to revolutionize some industrial applications, especially in separation, purification, and the storage of gases.[18-20] An ideal adsorbent for C_2H_2 separation is expected to be chemically stable, be able to capture trace C_2H_2 from C_2H_4 or other feed gas mixtures, and be able to regenerate easily. In recent years, a number of porous materials have been reported for C_2H_2/C_2H_4 separation through a synergistic approach of pore tuning and functionalization.[21,22] In 2016, Xing's group[14] reported the anion-pillared hybrid porous materials SIFSIX-2-Cu-i, with the specific binding sites and suitable pore space to effectively overcome the trade-off effect for C_2H_2 separation. In 2017, the first case of an ideal molecular sieve for C_2H_2/C_2H_4 was found called SIFSIX-14-Cu-i (UTSA-200),[23] which with the ultrafine tuning of its pore size (3.4 Å), can not only effectively block C_2H_4 but also adsorb high amounts of C_2H_2, thus setting up the benchmarks for both C_2H_2 adsorption and C_2H_2/C_2H_4 separation. However, UTSA-200 can also take up a large amount of CO_2 or C_3H_4 at the same conditions,[24,25] which significantly restricts its separation performance for C_2H_2/CO_2 and other multicomponent gases mixtures.

Traditional research on porous materials for gas separation mainly focused on those porous structures in the one-dimensional channel (Figure 1a) or cage type pore (Figure 1b). During our exploration of porous materials for C_2H_2 separation, we realized that one unique class of porous MOFs, which have interlayer pore cavities (Figure 1c)[26,27] in their layered structures, had been overlooked. Compared to the traditional pore types, this kind of pore cavity has a narrow pore space, may exhibit multiple host-guest interactions with gas molecules, and thus could be utilized for selective separation of some specific gas component.

Herein, we report an ultramicroporous MOF (Zn_2(bpy)(btec))[28,29] that incorporates two-dimensional interlayer cavities, which enabled the full entrance of C_2H_2 and effectively blocked the C_2H_4 and CO_2, thus exhibiting the benchmark C_2H_2/C_2H_4 and C_2H_2/CO_2 uptake ratios. According to the breakthrough experiments, C_2H_2 can be directly removed from C_2H_2/C_2H_4 (1/99, vol/vol) or C_2H_2/CO_2 (50/50, vol/vol) mixtures and high-purity C_2H_4 (>99.999%), CO_2 (>99.999%), and C_2H_2 (>98%) can be obtained in the single separation process. More importantly, Zn_2(bpy)(btec) can be straightforwardly synthesized at the kilogram scale under room temperature in an aqueous solution. Its good chemical stability, water stability, thermal stability, and cyclic stability are well satisfied requirements of industrial application.

2 | EXPERIMENTAL

2.1 | Synthesis of $[Zn_2(bpy)(btec)(H_2O)_2]\cdot 2H_2O$

2.1.1 | Hydrothermal synthesis

The synthesis of the crystal sample was performed following a reported method with minor modifications.[28] 0.1097 g (0.6 mmol) zinc acetate, 0.1091 g (0.5 mmol) pyromellitic dianhydride, 0.0781 g (0.5 mmol) 4,4′-bipyridine and 10 ml deionized water were well mixed in a 25 ml teflon-lined autoclave. Crystallization was carried out at 180°C for 5 days. Then the autoclaves are cooled to room temperature. The crystals were filtered off, washed with hot water/ethanol mixture (1:1) for three times, then dried in air (yield: 0.1306 g, 76.1% based on zinc acetate).

2.1.2 | Rapid room temperature synthesis

0.1527 g (0.7 mmol) pyromellitic dianhydride, 0.1093 g (0.7 mmol) 4,4′-bipyridine and 5 ml deionized water were mixed in a 20 ml sealed vial with stirring at ambient temperature for 10 min, then 200 μl $NH_3\cdot H_2O$ (25%) was added into the vial. After the above mixture was thoroughly mixed, a 5 ml aqueous solution of 0.2569 g (1.4 mmol) Zinc acetate was added with stirring for 10 min. Then the products were filtered off, washed with hot water/ethanol mixture (1:1) three times, then dried in air (yield: 0.3288 g, 82.1% based on 4,4′-bipyridine).

2.1.3 | Large-scale synthesis

Synthesis at the 1,000-times scale was carried out as follows. White powder sample was obtained by mixing an aqueous solution (0.65 L) of zinc acetate ($Zn[Ac]_2$, 1.64 mol, 0.3 kg) with an aqueous solution (1.10 L) of pyromellitic dianhydride (0.7 mol, 0.1528 kg), 4,4′-

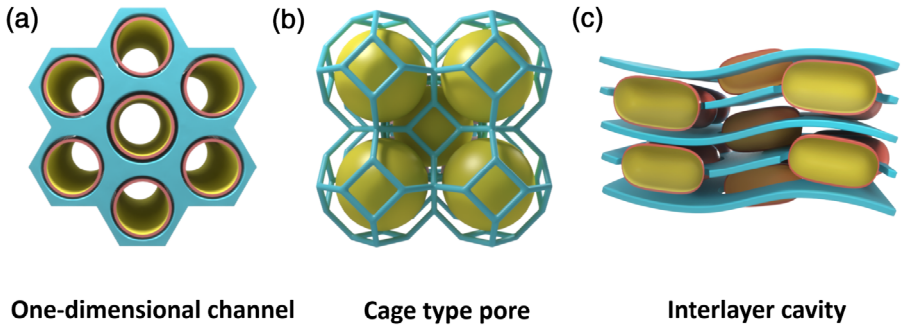

FIGURE 1 Schematic illustration of the representative porous structures in metal–organic frameworks (MOFs): (a) One-dimensional channel, (b) cage type pore, and (c) interlayer cavity [Color figure can be viewed at wileyonlinelibrary.com]

bipyridine (0.7 mol, 0.1094 kg) and 4 ml $NH_3{\cdot}H_2O$ (25%). The crystallization was finished at ambient temperature after stirring for 30 min, the sample was filtered, washed thoroughly with water/ethanol and dried under air, with a yield of 0.3236 kg (80.9% based on 4,4′-bipyridine).

2.2 | Characterization

The crystallinity and phase purity of the materials were measured by powder X-ray diffraction (PXRD) on a Bruker D8 ADVANCE X-ray diffractometer with Cu-Kα (λ = 1.5418 Å) radiation operated at 40 kV and 40 mA. Scanning was performed over the 2θ range of 5°–50° at 4°/min. Scanning electron microscopy (SEM) images were obtained using a Hitachi SEM (SU8010, Hitachi, Japan) equipped with a Horiba X-Max 50 EDX system. The thermogravimetric analysis (TGA) of the samples was collected on a thermal analyzer (NETZSCH, STA 449 F5) at a heating rate of 5°C/min under air atmosphere. CO_2 adsorption/desorption isotherms were obtained using an ASAP 2460 Surface Area and Porosity Analyzer at 273 K.

2.3 | Adsorption experiment

The purities of the acetylene, ethylene and carbon dioxide were higher than 99.99%. Their adsorption isotherms were collected with an Intelligent Gravimetric Analyser (IGA 001, Hiden, United Kingdom). Samples were activated under vacuum at 150°C overnight or until no further weight loss was observed. Adsorption equilibrium data was collected once a stable pressure (more than 20 adsorption points were recorded from 0 to 1 bar) and weight was maintained for at least 40 min to reach an adsorption equilibrium at each point along the isotherm.

2.4 | Breakthrough tests

The breakthrough experiments for C_2H_2/C_2H_4 (1/99, vol/vol) mixtures were carried out at a flow rate of 1.25 ml/min (298 K, 1.01 bar). In the separation experiment, Zn_2(bpy)(btec) sample (3.0575 g) was packed into Φ 4 × 275 mm stainless steel column, and the column was activated under reduced pressure at 150°C overnight. The experimental set-up consisted of two fixed-bed stainless steel reactors. One reactor was loaded with the adsorbent, while the other reactor was used as a blank control group to stabilize the gas flow. The horizontal reactors were placed in a temperature-controlled environment, maintained at 298 K. The flow rates of all gas mixtures were regulated by mass flow controllers, and the effluent gas stream from the column was monitored by gas chromatography. Prior to the breakthrough experiment, we activated the sample by flushing the adsorption bed with helium gas for 2 hr at 150°C. Subsequently, the column was allowed to equilibrate at the measurement rate before we switched the gas flow.

3 | RESULTS AND DISCUSSION

3.1 | Structure characterization

The synthesized $[Zn_2(bpy)(btec)(H_2O)_2]{\cdot}2H_2O$ has a two-dimensional structure, each layer is formed by Zn coordinated with bpy and btec, and H_2O molecules between layers provide multiple hydrogen bonding sites to connect the two layers.[28] In this work, we investigated the rapid synthesis and large-scale synthesis processes of these materials, the PXRD patterns of these samples were matched well with the simulated one, and the SEM images show that the samples have relatively high crystallinity (Figures S1 and S2). After guest removal, Zn_2(bpy)(btec) still shows porosity with the pore cavities of 3.6 Å × 3.8 Å × 6.6 Å (Figure 2). These cavities match well with the size and shape of C_2H_2 (3.3 Å × 3.3 Å × 5.7 Å), suggesting a potential application for C_2H_2 separation.

The porosity in Zn_2(bpy)(btec) was established by CO_2 sorption at 273 K. As shown in Figure S3, the CO_2 adsorption isotherms slowly increase with increasing pressure. By using the Dubinin–Radushkevich equation, the surface area of Zn_2(bpy)(btec) was calculated to be 397 m^2/g, and its pore-size is around 3.6 Å (Figure S3). The pore cavity between two layers is about 3.6 Å × 3.8 Å × 6.6 Å, which is slightly larger than the size of C_2H_2, CO_2 and smaller than C_2H_4, thus could be used for C_2H_2/C_2H_4 and C_2H_2/CO_2 separation.

3.2 | Single-gas sorption isotherm

Pure component equilibrium adsorption isotherms for C_2H_2, C_2H_4 and CO_2 were measured at 298 K up to 1 bar, as presented in Figure 3a. The C_2H_2 uptake on Zn_2(bpy)(btec) reached 93.5 cm^3/cm^3 at 298 K and 1 bar, significantly higher than that of C_2H_4 and CO_2 at the same conditions. Notably, through size sieving by the appropriate aperture, Zn_2(bpy)(btec) presents the C_2H_2 uptake of 93.5 cm^3/cm^3, very low C_2H_4 uptake of 9.1 cm^3/cm^3 and low CO_2 uptake of 28.9 cm^3/cm^3 (298 K and 1 bar), giving an excellent uptake ratio of C_2H_2 over C_2H_4 (10.31) and CO_2 (3.23), which are the highest values among the indicated MOFs (Tables S2 and S3).

To compare the separation properties of Zn_2(bpy)(btec) with other top-performing MOFs, its ideal adsorbed solution theory (IAST) selectivity of C_2H_2 over C_2H_4 and CO_2 were calculated on their single-component isotherms (Figure 3a). The gas mixtures were selected as C_2H_2/C_2H_4 (1:99, vol/vol) and C_2H_2/CO_2 (50:50, vol/vol) at a total gas pressure of 1 bar and 298 K, to mimic the composition of the industrial purification process. As seen in Figure 3b,c, Zn_2(bpy)(btec) exhibits an extraordinarily high selectivity of over 107.8 for the C_2H_2/C_2H_4 mixture and 33.3 for the C_2H_2/CO_2 mixture, notably higher than the previous benchmark SIFSIX-2-Cu-i (44.54),[14] M′MOF-3a (24.03),[30] CPL-1 (26.8)[31] and ELM-12 (14.8)[32] for C_2H_2/C_2H_4 separation, and FeNi-M'MOF (24)[33] HOF-3a (21),[34] UTSA-74 (9),[35] TIFSIX-2-Cu-i (6.5)[36] and for C_2H_2/CO_2 separation.

In industrial applications, energy cost in the regeneration process is also an unavoidable problem and should be taken into

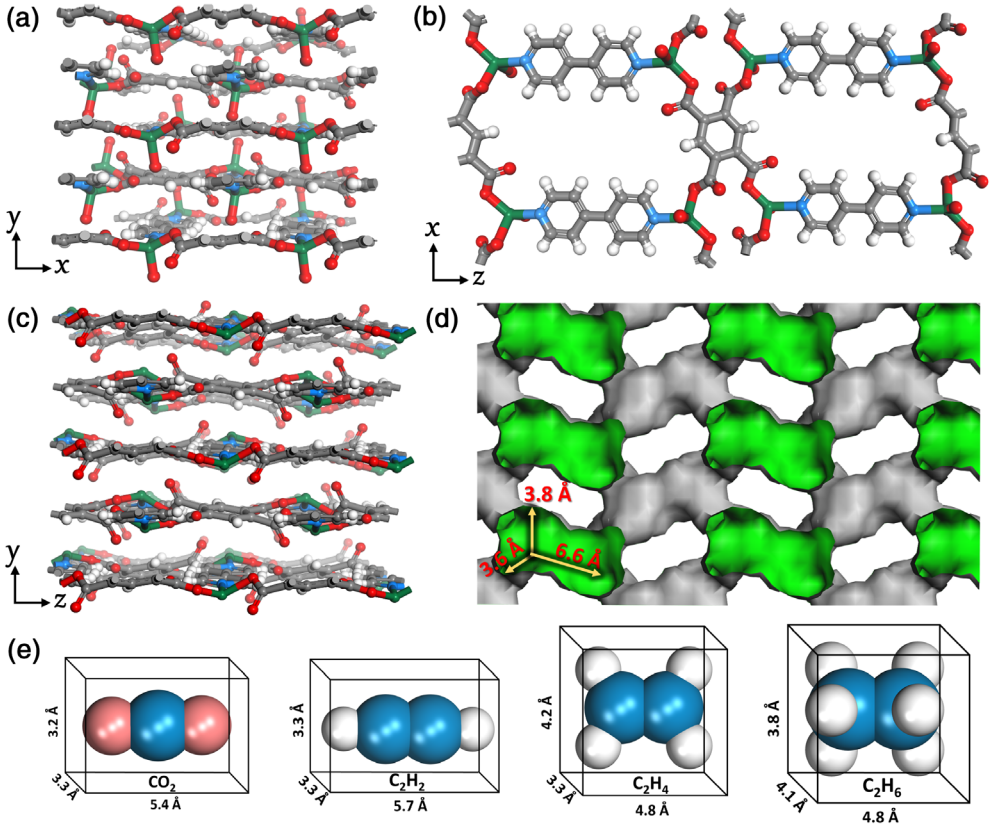

FIGURE 2 (a–c) The crystal structures of Zn_2(bpy)(btec). (d) The channel shapes and pore cavity size of Zn_2(bpy)(btec). (e) Comparison of molecular size difference of C_2H_2, C_2H_4,C_2H_6 and CO_2(Color code: Zn, green; O, red; N, light blue; C, gray) [Color figure can be viewed at wileyonlinelibrary.com]

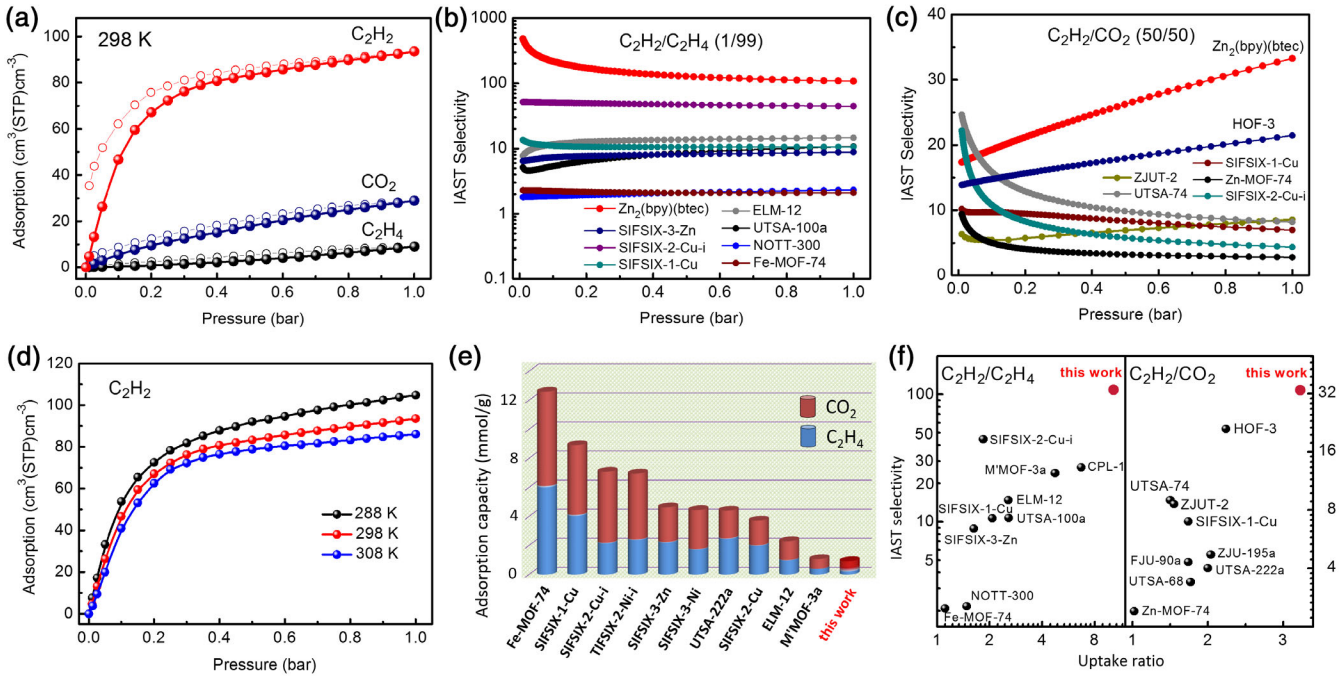

FIGURE 3 (a) Single-component sorption isotherms of C_2H_2, C_2H_4, and CO_2 at 298 K for Zn_2(bpy)(btec). (b, c) Ideal adsorbed solution theory (IAST) selectivities of C_2H_2/C_2H_4 (1/99) and C_2H_2/CO_2 (50/50) mixtures on some benchmark materials. (d) Adsorption isotherms of C_2H_2 for Zn_2(bpy)(btec) at 288–308 K. (e) C_2H_4 and CO_2 uptakes of different metal–organic framework (MOF) materials at 1 bar and 298 K. (f) Comparison of C_2H_2/C_2H_4 (1/99) and C_2H_2/CO_2 (50/50) IAST selectivities and C_2H_2—C_2H_4—CO_2 uptake ratios of different adsorbents at 1 bar and 298 K [Color figure can be viewed at wileyonlinelibrary.com]

consideration. The interactions between the adsorbents and C_2H_2 are evaluated by calculating the isosteric heats of adsorption (Q_{st}), which is measured from the single component isotherms at different temperatures (Figure 3d). The calculated Q_{st} of Zn_2(bpy)(btec) at zero coverage for C_2H_2, C_2H_4, and CO_2 are 28.7, 26.3, and 24.8 kJ/mol (Figure S4), respectively, which is much lower than those values reported in other MOFs with open metal sites such as MOF-74 series (47 kJ/mol (C_2H_2) for Fe-MOF-74).[12] Thus, the molecular sieving based adsorption not only avoided excessive temperature fluctuations during the adsorption process but also decreased the cost and energy requirement in the regeneration process, which indicates advantages of Zn_2(bpy)(btec) in real industrial applications. In addition, comparing with other top-performing materials (Tables S2 and S3), Zn_2(bpy)(btec) exhibits the lowest total C_2H_4 and CO_2 loading in normal conditions (Figure 3e), and less co-adsorption will lead to a higher C_2H_2 purity in the generation process. Besides, this material exhibits the highest C_2H_2/C_2H_4 uptake ratio (10.31) and C_2H_2/CO_2 uptake ratio (3.23), as well as extraordinarily high selectivity (107.8, 33.3) (Figure 3f), which makes it one of the most promising materials for the efficient C_2H_2 separation from C_2H_4 or CO_2 mixtures.

3.3 | Breakthrough separation

Furthermore, we performed actual breakthrough experiments on Zn_2(bpy)(btec) to establish the feasibility of C_2H_2/C_2H_4 and C_2H_2/CO_2 separations, in which C_2H_2/C_2H_4 (vol/vol, 1/99) and C_2H_2/CO_2 (vol/vol, 50/50) mixtures were used as feeds to mimic the industrial process conditions (Figures 4 and S6). As shown in Figure 4a,c, only after several minutes, C_2H_4 or CO_2 first eluted through the bed to yield a polymer-grade gas and the purity of C_2H_4 monitored at the outlet was >99.999%. Then, after a long period of time (130 min for C_2H_2/C_2H_4, 50 min for C_2H_2/CO_2), C_2H_2 broke through from the adsorption bed. During this process, C_2H_2 was clearly captured by Zn_2(bpy)(btec), with the concentration of the impurities decreased to lower than 1 ppm for C_2H_4 and 10 ppm for CO_2. Polymer-grade C_2H_4 and high purity of CO_2 were directly collected at the outlet. From the desorption curves in Figure 4b,d, it can be found that adsorbates were fully desorbed from the materials in 20 min. Due to the high C_2H_2/C_2H_4 and C_2H_2/CO_2 uptake ratios and selectivities, a high purity of C_2H_2 over 98.5% (b) or 92.5% (d) were generated, respectively.

The kinetic ad/desorption rate of C_2H_2 was also investigated in Figures S8 and S9, showing that Zn_2(bpy)(btec) has a high kinetic ad/desorption rate, and therefore that C_2H_2 can be saturated or fully desorbed in about 10 min. In addition, the desorption and recycling measurements revealed that this material can maintain its C_2H_2 capture ability and high selectivity in several repeated adsorption and separation cycles (Figures 4b,d and S7). The breakthrough time remains almost unchanged during five cyclic breakthrough experiments, confirming the good recyclability of this material for the C_2H_2/C_2H_4 and C_2H_2/CO_2 separation.

Generally, in the real production process, the feed gas also contains some other components, which is a tremendous challenge in the recovery of C_2H_2 from such refinery gas. Therefore, we investigated the single-component adsorption isotherms of some main components of refinery gas (CH_4, C_2H_2, C_2H_4, C_2H_6, C_3H_4, C_3H_6 and C_3H_8) and common gas components (CO_2, H_2, N_2 and O_2) as seen in Figure 5a,b. Based on the well-matched pore cavity of Zn_2(bpy)(btec),

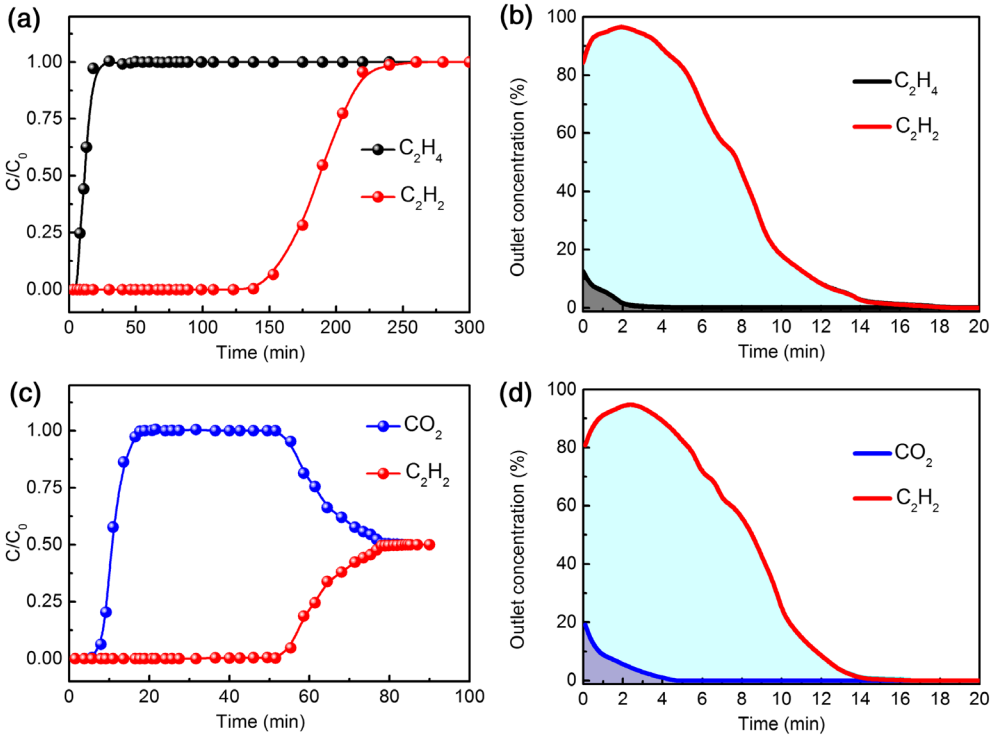

FIGURE 4 Experimental breakthrough (298 K, 1 bar) and desorption (333 K, 1 bar) curves for C_2H_2/C_2H_4 (1/99) (a, b) and C_2H_2/CO_2 (50/50) (c, d) mixtures on Zn_2(bpy)(btec) [Color figure can be viewed at wileyonlinelibrary.com]

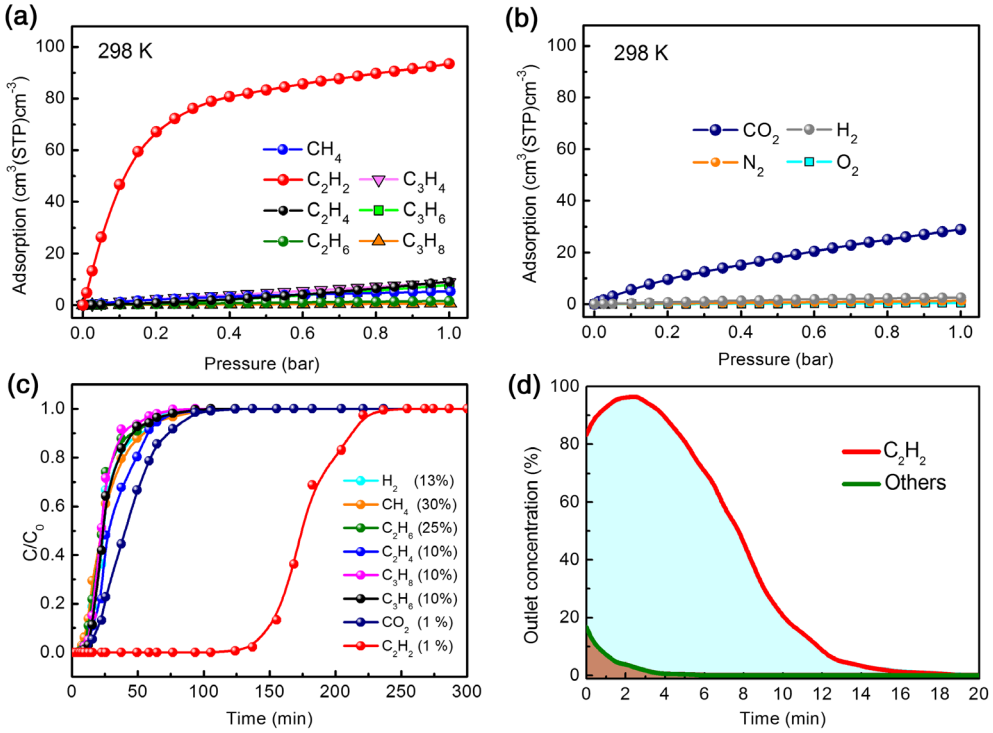

FIGURE 5 (a, b) Single-component adsorption isotherms of CH_4, C_2H_2, C_2H_4, C_2H_6, C_3H_4, C_3H_6, C_3H_8, CO_2, H_2, O_2, and N_2 in Zn_2(bpy)(btec) at 298 K. (c, d) Multi-component breakthrough (298 K, 1 bar) and desorption (333 K, 1 bar) curves for CH_4/C_2H_2/C_2H_4/C_2H_6/C_3H_6/C_3H_8/CO_2/H_2 (30/1/10/25/10/10/1/13) mixtures on Zn_2(bpy)(btec) [Color figure can be viewed at wileyonlinelibrary.com]

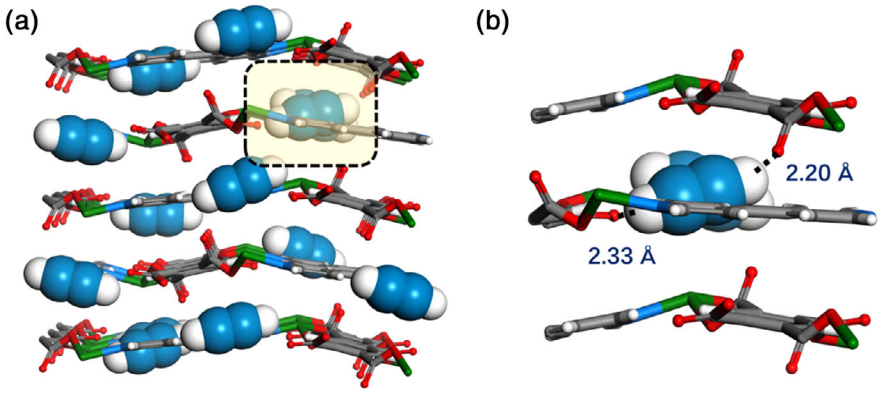

FIGURE 6 Calculated C_2H_2 molecule binding sites in Zn_2(bpy)(btec) by grand canonical Monte Carlo (GCMC) simulation. Color code: Zn (green), O (red), N (light blue), C (gray), and C_2H_2 (blue) [Color figure can be viewed at wileyonlinelibrary.com]

this material selectively adsorbs C_2H_2 and blocks most other molecules to achieve an admirable sieving effect. The uptakes of most of the gases were below 10 cm^3/cm^3 at 1 bar and 298 K. Furthermore, the gas mixtures separation process was carried out on this molecular sieve material for the recovery of C_2H_2 from the simulated steam cracking mixtures. As can be seen from the breakthrough curves (Figure 5c), most of the mixture gases eluted through the fixed bed quickly and a trace amount of C_2H_2 was totally adsorbed during the long retention time. The calculated C_2H_2/C_2H_4 and C_2H_2/CO_2 separation selectivities from the multi-component breakthrough curve were 9.7 and 5.1,[37] which indicated the good C_2H_2 separation abilities of Zn_2(bpy)(btec) under dynamic conditions. In the generation process (Figure 5d), the adsorbent was fully desorbed in 20 min and obtained high purity C_2H_2 (>98%). The multi-component separation and desorption tests show strong evidence of the efficient C_2H_2 separation ability of Zn_2(bpy)(btec) materials, which has initiated the promise of MOF materials for this very important industrial application.

3.4 | Grand canonical Monte Carlo simulations

To have a better insight into the excellent C_2H_2 separation ability of Zn_2(bpy)(btec), grand canonical Monte Carlo (GCMC) simulations were performed to structurally elucidate how C_2H_2 molecules are adsorbed in this MOF.[35,38,39] The calculated binding sites of C_2H_2 are shown in Figure 6. The C_2H_2 molecules are preferentially located in the pore cavities between the layers of Zn_2(bpy)(btec). The C—H···O hydrogen bonds of each C_2H_2 molecule interacts with two oxygen molecule with a distance of 2.2–2.33 Å, which are much shorter than the sum of the van der Waals radii of oxygen (1.52 Å) and hydrogen (1.20 Å) atoms, indicating a relatively strong interaction.

3.5 | Scalable synthesis and stability

In order to promote the industrialization of MOFs materials, it is the general trend to produce stable MOF materials at low costs and with

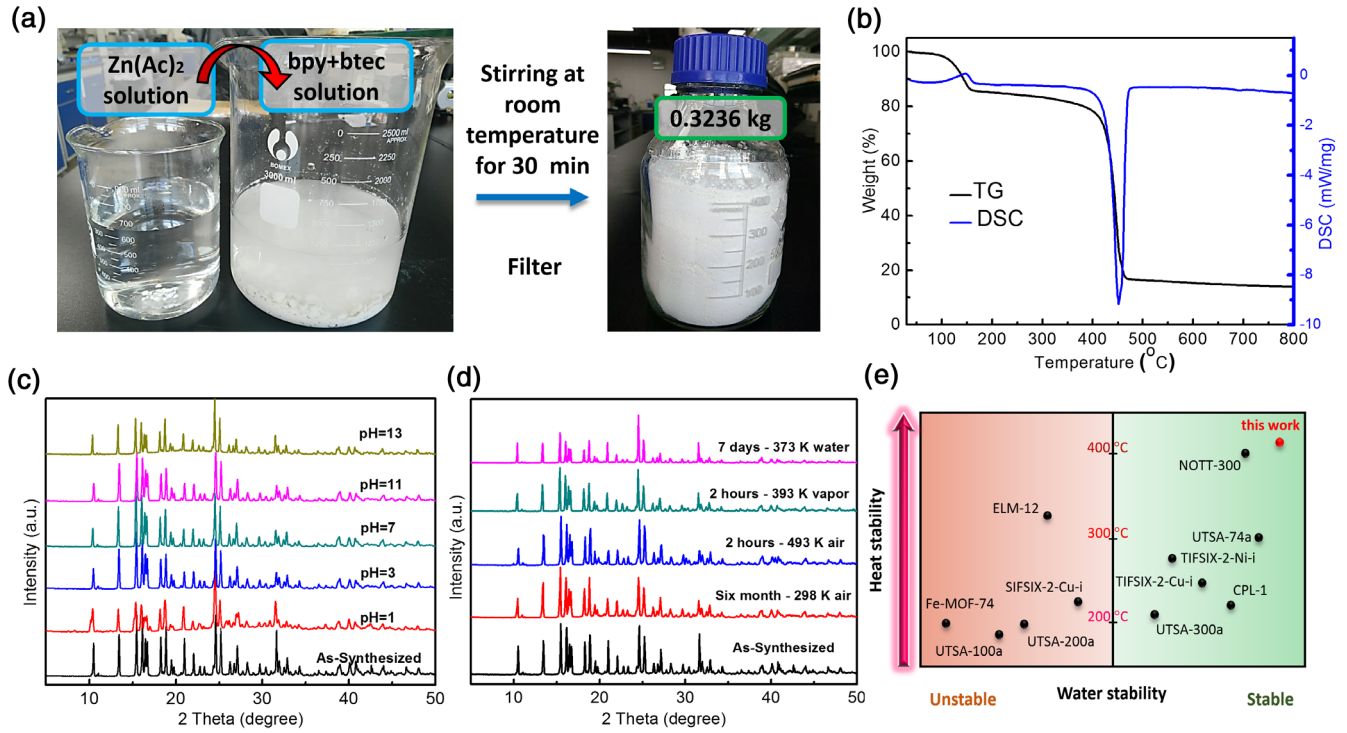

FIGURE 7 (a) Scale-up synthesis of $[Zn_2(bpy)(btec)(H_2O)_2]\cdot 2H_2O$. (b) Thermogravimetric and differential scanning calorimetry (DSC) curves for as-synthesized $[Zn_2(bpy)(btec)(H_2O)_2]\cdot 2H_2O$. (c, d) Powder X-ray diffraction (PXRD) patterns of $[Zn_2(bpy)(btec)(H_2O)_2]\cdot 2H_2O$ after different treatment. (e) Comparison of the heat and water stability of some benchmark metal–organic framework (MOF) materials [Color figure can be viewed at wileyonlinelibrary.com]

simple operation processes. Therefore, a water-based and scalable synthesis was developed at room temperature for the large-scale preparation of $[Zn_2(bpy)(btec)(H_2O)_2]\cdot 2H_2O$. As shown in Figure 7a, only by mixing the metal salt and the ligands in aqueous solution and stirring for 30 min, then filtering and drying, can we obtain more than 320 g of product at room temperature. TGA and differential scanning calorimetry (DSC) were tested on $[Zn_2(bpy)(btec)(H_2O)_2]\cdot 2H_2O$ to explore its thermal stabilities (Figure 7b). Below 150°C, the initial weight loss of ~14% was accounted for by the loss of water molecules, and then $Zn_2(bpy)(btec)$ can stabilize up to about 410°C before its decomposition.

Besides, the adsorbents require relatively high thermostability to keep a long operation lifetime, the real C_2H_2-relevant separation tasks are typically implemented under more extreme conditions, typically containing a trace amount of water and acidic gases.[40] Herein, the structural stability of $Zn_2(bpy)(btec)$ was examined in detail. As depicted in Figure 7c,d, the PXRD patterns of those materials treated under extreme conditions (acid, base, or boiling water) coincide with those of pristine samples, which indicates that its structure has no framework collapse and still retains its crystallinity. After such treatment, its C_2H_2 adsorption is largely maintained, comparable to the initial value (Figures S10 and S11), which demonstrated that this material is very stable in the acidic/basic solutions (pH = 1–13), even in the water up to 120°C. The water and thermal stability of $Zn_2(bpy)(btec)$ has been superior to most C_2H_2-separated MOFs (Figure 7e). Its exceptionally high stability is due to its dense structure forming by the strong multiple hydrogen bonding interactions and offset π-π stacking interactions (Figure S12).

4 | CONCLUSION

In summary, we have identified an abnormally layered MOF ($Zn_2(bpy)(btec)$) for the highly efficient separation of C_2H_2 from C_2H_4 and CO_2 mixtures. The interlayer pores cavity can exactly adsorb C_2H_2 and block C_2H_4 or the other C1—C3 hydrocarbons, resulting in by far both the highest C_2H_2/C_2H_4 and C_2H_2/CO_2 uptake ratios (10.31, 3.23) and superior IAST selectivities (107.8, 33.3) among the rigid MOFs. Through size sieving by the appropriate aperture, this MOF achieves efficient separation of C_2H_2/C_2H_4 (1/99, vol/vol), C_2H_2/CO_2 (50/50, vol/vol) and simulated steam cracking mixtures, finally obtaining a polymer grade of C_2H_4 (99.999%) and a high purity of C_2H_2 (98%). Furthermore, the synthesis of this material is easily scale-up at an environmentally friendly condition and its structure can be maintained in solutions with a wide range of pH (1–13) as well as in the boiling (373 K) water. These desirable properties of $Zn_2(bpy)(btec)$ demonstrated that this new MOF material is a promising adsorbent, which has great potential to be used for the practical C_2H_2 production process.

ACKNOWLEDGMENTS

We gratefully acknowledge the financial support from the National Natural Science Foundation of China (No. 21908155, 21922810 and 21878205), Natural Science Foundation for Young Scientists of Shanxi Province (No. 201901D211053).

AUTHOR CONTRIBUTIONS

Yang Chen: Conceptualization; funding acquisition; investigation; writing-original draft. **Yadan Du:** Data curation; investigation. **Yong Wang:** Data curation; investigation. **Rajamani Krishna:** Formal analysis; investigation. **Libo Li:** Conceptualization; funding acquisition; resources; writing-review and editing. **Jiangfeng Yang:** Formal analysis. **Jinping Li:** Resources; supervision. **Bin Mu:** Conceptualization; writing-review and editing.

CONFLICT OF INTEREST

The authors declare no conflict of interest.

ORCID

Yang Chen https://orcid.org/0000-0001-5743-4182
Rajamani Krishna https://orcid.org/0000-0002-4784-8530
Libo Li https://orcid.org/0000-0001-7147-9838
Jinping Li https://orcid.org/0000-0002-2628-0376
Bin Mu https://orcid.org/0000-0002-9117-1299

REFERENCES

1. Chen K-J, Madden DG, Mukherjee S, et al. Synergistic sorbent separation for one-step ethylene purification from a four-component mixture. *Science*. 2019;366(6462):241-246.
2. Hu TL, Wang H, Li B, et al. Microporous metal-organic framework with dual functionalities for highly efficient removal of acetylene from ethylene/acetylene mixtures. *Nat Commun*. 2015;6:7328.
3. Wang J, Xie D, Zhang Z, et al. Efficient adsorption separation of acetylene and ethylene via supported ionic liquid on metal-organic framework. *AIChE J*. 2016;63(6):2165-2175.
4. Matsuda R, Kitaura R, Kitagawa S, et al. Highly controlled acetylene accommodation in a metal-organic microporous material. *Nature*. 2005;436(7048):238-241.
5. Pei J, Shao K, Wang JX, et al. A chemically stable Hofmann-type metal-organic framework with sandwich-like binding sites for benchmark acetylene capture. *Adv Mater*. 2020;32:e1908275.
6. Li J, Jiang L, Chen S, et al. Metal-organic framework containing planar metal-binding sites: efficiently and cost-effectively enhancing the kinetic separation of C_2H_2/C_2H_4. *J Am Chem Soc*. 2019;141(9):3807-3811.
7. Belmabkhout Y, Zhang Z, Adil K, et al. Hydrocarbon recovery using ultra-microporous fluorinated MOF platform with and without uncoordinated metal sites: I- structure properties relationships for C_2H_2/C_2H_4 and CO_2/C_2H_2 separation. *Chem Eng J*. 2019;359:32-36.
8. Li JR, Kuppler RJ, Zhou HC. Selective gas adsorption and separation in metal-organic frameworks. *Chem Soc Rev*. 2009;38(5):1477-1504.
9. Foo ML, Matsuda R, Hijikata Y, et al. An adsorbate discriminatory gate effect in a flexible porous coordination polymer for selective adsorption of CO_2 over C_2H_2. *J Am Chem Soc*. 2016;138(9):3022-3030.
10. Sholl DS, Lively RP. Seven chemical separations to change the world. *Nature*. 2016;532(7600):435-437.
11. Zhao X, Yang Q, Xu D, et al. Design and screening of ionic liquids for C_2H_2/C_2H_4 separation by COSMO-RS and experiments. *AIChE J*. 2015;61(6):2016-2027.
12. Bloch ED, Queen WL, Krishna R, Zadrozny JM, Brown CM, Long JR. Hydrocarbon separations in a metal-organic framework with open iron(II) coordination sites. *Science*. 2012;335(6076):1606-1610.
13. He Y, Xiang S, Chen B. A microporous hydrogen-bonded organic framework for highly selective C_2H_2/C_2H_4 separation at ambient temperature. *J Am Chem Soc*. 2011;133(37):14570-14573.
14. Cui X, Chen K, Xing H, et al. Pore chemistry and size control in hybrid porous materials for acetylene capture from ethylene. *Science*. 2016;353(6295):141-144.
15. Férey G, Serre C, Devic T, et al. Why hybrid porous solids capture greenhouse gases? *Chem Soc Rev*. 2011;40(2):550-562.
16. Chen Z, Li P, Anderson R, et al. Balancing volumetric and gravimetric uptake in highly porous materials for clean energy. *Science*. 2020;368(6488):297-303.
17. Rieth AJ, Wright AM, Dincă M. Kinetic stability of metal–organic frameworks for corrosive and coordinating gas capture. *Nat Rev Mater*. 2019;4:708-725.
18. Liao P-Q, Huang N-Y, Zhang W-X, Zhang J-P, Chen X-M. Controlling guest conformation for efficient purification of butadiene. *Science*. 2017;356(6343):1193-1196.
19. Shan B, Yu J, Armstrong MR, et al. A cobalt metal-organic framework with small pore size for adsorptive separation of CO_2 over N_2 and CH_4. *AIChE J*. 2017;63(10):4532-4540.
20. Yang S, Ramirez-Cuesta AJ, Newby R, et al. Supramolecular binding and separation of hydrocarbons within a functionalized porous metal-organic framework. *Nat Chem*. 2014;7(2):121-129.
21. Furukawa H, Ko N, Go YB, et al. Ultrahigh porosity in metal-organic frameworks. *Science*. 2010;329(5990):424-428.
22. Lv D, Chen J, Chen Y, et al. Moisture stability of ethane-selective Ni(II), Fe(III), Zr(IV)-based metal-organic frameworks. *AIChE J*. 2019;65(8):e16616.
23. Li B, Cui X, O'Nolan D, et al. An ideal molecular sieve for acetylene removal from ethylene with record selectivity and productivity. *Adv Mater*. 2017;29:1704210.
24. Jiang M, Li B, Cui X, et al. Controlling pore shape and size of interpenetrated anion-pillared ultramicroporous materials enables molecular sieving of CO_2 combined with ultrahigh uptake capacity. *ACS Appl Mater Interfaces*. 2018;10(19):16628-16635.
25. Li L, Wen H-M, He C, et al. A metal-organic framework with suitable pore size and specific functional sites for the removal of trace propyne from propylene. *Angew Chem Int Ed*. 2018;57(46):15183-15188.
26. Lin RB, Li L, Wu H, et al. Optimized separation of acetylene from carbon dioxide and ethylene in a microporous material. *J Am Chem Soc*. 2017;139(23):8022-8028.
27. Li L, Lin R-B, Krishna R, et al. Flexible-robust metal-organic framework for efficient removal of propyne from propylene. *J Am Chem Soc*. 2017;139(23):7733-7736.
28. Wu C-D, Lu C-Z, Wu D-M, Zhuang H-H, Huang J-S. Hydrothermal synthesis of two new zinc coordination polymers with mixed ligands. *Inorg Chem Commun*. 2001;4(10):561-564.
29. Yang S-Y, Sun Z-G, Long L-S, Huang R-B, Zheng L-S. Crystal structure of a 2D coordination polymer: dizinc pyromellitate 4, 4′-bipyridine tetrahydrate. *Main Group Met Chem*. 2002;25(11):699-700.
30. Xiang SC, Zhang Z, Zhao CG, et al. Rationally tuned micropores within enantiopure metal-organic frameworks for highly selective separation of acetylene and ethylene. *Nat Commun*. 2011;2:204.
31. Zheng F, Guo L, Gao B, et al. Engineering the pore size of pillared-layer coordination polymers enables highly efficient adsorption separation of acetylene from ethylene. *ACS Appl Mater Interfaces*. 2019;11(31):28197-28204.
32. Li L, Lin R-B, Krishna R, et al. Efficient separation of ethylene from acetylene/ethylene mixtures by a flexible-robust metal-organic framework. *J Mater Chem A*. 2017;5:18984-18988.

33. Gao J, Qian X, Lin RB, et al. Mixed metal-organic framework with multiple binding sites for efficient C_2H_2/CO_2 separation. *Angew Chem Int Ed*. 2020;59(11):4396-4400.
34. Li P, He Y, Zhao Y, et al. A rod-packing microporous hydrogen-bonded organic framework for highly selective separation of C_2H_2/CO_2 at room temperature. *Angew Chem Int Ed*. 2015;54(2):574-577.
35. Luo F, Yan C, Dang L, et al. UTSA-74: a MOF-74 isomer with two accessible binding sites per metal center for highly selective gas separation. *J Am Chem Soc*. 2016;138(17):5678-5684.
36. Chen K-J, Scott Hayley S, Madden David G, et al. Benchmark C_2H_2/CO_2 and CO_2/C_2H_2 separation by two closely related hybrid ultramicroporous materials. *Chem*. 2016;1(5):753-765.
37. Lin RB, Li L, Zhou HL, et al. Molecular sieving of ethylene from ethane using a rigid metal-organic framework. *Nat Mater*. 2018;18(12):1128-1133.
38. Hao HG, Zhao YF, Chen DM, et al. Simultaneous trapping of C_2H_2 and C_2H_6 from a ternary mixture of $C_2H_2/C_2H_4/C_2H_6$ in a robust metal-organic framework for the purification of C_2H_4. *Angew Chem Int Ed*. 2018;57(49):16067-16071.
39. Zhang C, Wang L, Maurin G, Yang Q. In silico screening of MOFs with open copper sites for C_2H_2/CO_2 separation. *AIChE J*. 2018;64(11):4089-4096.
40. Weissermel K, Arpe H-J. *Industrial Organic Chemistry*. 4th ed. Weinheim, Germany: Wiley-VCH; 2003.

SUPPORTING INFORMATION

Additional supporting information may be found online in the Supporting Information section at the end of this article.

How to cite this article: Chen Y, Du Y, Wang Y, et al. A stable metal–organic framework with well-matched pore cavity for efficient acetylene separation. *AIChE J*. 2021;67:e17152. https://doi.org/10.1002/aic.17152

Supporting Information

A stable metal–organic framework with well-matched pore cavity for efficient acetylene separation

Yang Chen,[a] Yadan Du,[a] Yong Wang,[a] Rajamani Krishna,[b] Libo Li,[a,c,*] Jiangfeng Yang, [a,c]

Jinping Li, [a,c] and Bin Mu[d,*]

[a]College of Chemistry and Chemical Engineering, Shanxi Key Laboratory of Gas Energy Efficient and Clean Utilization, Taiyuan University of Technology, Taiyuan 030024, Shanxi, P. R. China

[b]Van 't Hoff Institute for Molecular Sciences, University of Amsterdam, Science Park 904, 1098 XH Amsterdam, The Netherlands

[c]Key Laboratory of Coal Science and Technology, Ministry of Education and Shanxi Province, Taiyuan University of Technology, Taiyuan 030024, Shanxi, P. R. China

[d]Chemical Engineering, School for Engineering of Matter, Transport, and Energy, Arizona State University, Tempe, Arizona, 85287, United States

*Corresponding author:

Libo Li (lilibo908@hotmail.com)

Bin Mu (bmu@asu.edu)

Table of Contents

1. Materials and stability test……S3

1.1 Materials……S3

1.2 Stability test……S3

2. Calculation details……S3

2.1 Fitting of pure component isotherms……S3

2.2 IAST calculations of adsorption selectivity……S4

2.3 Isosteric heat of adsorption……S4

2.4 Kinetic adsorption rate……S5

2.5 GCMC simulations……S5

3. PXRD and Morphology characterization of samples……S6

4. Adsorption and pore characterization……S7

5. Fitting of pure component isotherms……S8

6. Breakthrough experiment apparatus……S9

7. Kinetic adsorption and desorption test……S10

8. Stability of C_2H_2 adsorption……S11

9. Structure chart and calculate parameters……S12

10. Comparison of parameters for various MOFs……S13

11. References……S15

1. Materials and stability test

1.1 Materials

All the reagents were used without further purification. Zinc acetate ($Zn(AC)_2$, 99.0%), Pyromellitic dianhydride (btec, 99.0%) and 4,4'-Bipyridine (bpy, 98.0%) were purchased from Aladdin Reagent Co. Ltd. Ammonia solution ($NH_3•H_2O$, 25%) and ethanol was obtained from Sinopharm Group Chemical Reagent Co., Ltd. The deionized water was purified by using a Millipore Elix Advantage 3 purification system.

1.2 Stability test and comparison

The chemical stability of Zn_2(bpy)(btec) is investigated as follows: Zn_2(bpy)(btec) powder sample was immersed in water, HCl (pH = 1 to 3) and NaOH (pH = 7 to 13) solutions for 6 h, respectively. After that, samples were washed with water and dried in air. Water stability of samples was investigated using liquid water (298 K for 6 months, 373 K for 7 days) and water vapor (393 K for 2 hours) under different conditions. Thermal stability test was conducted at 493 K for 2 hours, then cool naturally in the air.

The PXRD patterns of Zn_2(bpy)(btec) treated under different conditions were coincide with the pristine samples (Figure 7c, d), which indicate that Zn_2(bpy)(btec) has no framework collapse and still retains its crystallinity.

The water stability sequence is based on the test results of water stability and acid-base stability in aqueous solutions reported in the literatures. The thermal stability sequence is based on the thermal stability test of the reported materials and their thermogravimetric data (Fig. 7e, Table S2, and S3).

2. Calculation details

2.1 Fitting of experimental data on pure component isotherms

The isotherm data for C_2H_2, C_2H_4, and CO_2 in Zn_2(bpy)(btec) were measured at 298 K. The data were fitted with the 1-site Langmuir-Freundlich model

$$q = q_{sat}\frac{bp^{v}}{1+bp^{v}} \quad (1)$$

The corresponding fitting parameters are provided in Table S1.

2.2 Calculations of selectivities

The selectivity of binary 1/99 C_2H_2/C_2H_4, and 50/50 C_2H_2/CO_2 mixtures in Zn_2(bpy)(btec) at 298 K were calculated by IAST method. Adsorption selectivity is defined by

$$S_{ads} = \frac{q_1/q_2}{p_1/p_2} \quad (2)$$

Where q_1 and q_2 are the *absolute* component loadings of the adsorbed phase in the mixture, and p_1 and p_2 are the component partial pressures. The component loadings and adsorption selectivity S_{ads} for 1/99 C_2H_2/C_2H_4 and 50/50 C_2H_2/CO_2 mixtures in Zn_2(bpy)(btec) at 298 K were determined using IAST.

The separation selectivity from multi-component breakthrough curve is reflected in the selectivity of mixed gases during dynamic adsorption, defined as

$$S_{sep} = \frac{n_1/c_1}{n_2/c_2} \quad (3)$$

Where n_1 and n_2 are captured amount of gas component during the breakthrough process in Zn_2(bpy)(btec).[1] C_1 and C_2 are the concentration of gas component in mixed gases.

2.3 Isosteric heat of adsorption

The binding energy of C_2H_2 in the MOFs is reflected in isosteric heat of adsorption, Q_{st}, defined as

$$Q_{st} = RT^2 \left(\frac{\partial \ln p}{\partial T} \right)_q \tag{4}$$

The calculations are based on the use of the Clausius-Clapeyron equation. The values for Zn_2(bpy)(btec) are determined by the adsorption data measured from 0~1 bar at 288, 298 and 308 K, respectively.

2.4 Kinetic adsorption rate

Diffusional time constants (D', D/r^2) were calculated by the short-time solution of the diffusion equation assuming a step change in the gas-phase concentration, clean beds initially, and micropore diffusion control:

$$\frac{q_t}{q_\infty} = \frac{6}{\sqrt{\pi}} \bullet \sqrt{\frac{D \bullet t}{r^2}} \tag{5}$$

Where q_t is the gas uptake at time t, q_∞ is the gas uptake at equilibrium, D is the diffusivity and r is the radius of the equivalent spherical particle. The slopes of q_t/q_∞ versus $\sqrt{t}$ are derived from the fitting of the plots in the low gas uptake range.

2.5 GCMC simulations

Grand canonical Monte Carlo (GCMC) simulations were performed to study the C_2H_2 adsorption on Zn_2(bpy)(btec) at 298 K and 1 bar. In this work, the adsorption sites of Zn_2(bpy)(btec) were estimated using a literature procedure.[2,3] The Zn_2(bpy)(btec) is treated as rigid with atoms frozen at their crystallographic positions during GCMC simulations. The GCMC calculations were performed using the Sorption code in Materials Studio. Simulation module was on the basis of the force field of COMPASS. A simulation box containing 8 (2 × 2 × 2) unit cells was built in this work. A cutoff radius was set to 12 Å for the Lennard−Jones interactions. For each state point, the GCMC simulation consists of 1.0×10^7 steps to guarantee the equilibration.

3. PXRD and Morphology characterization of samples

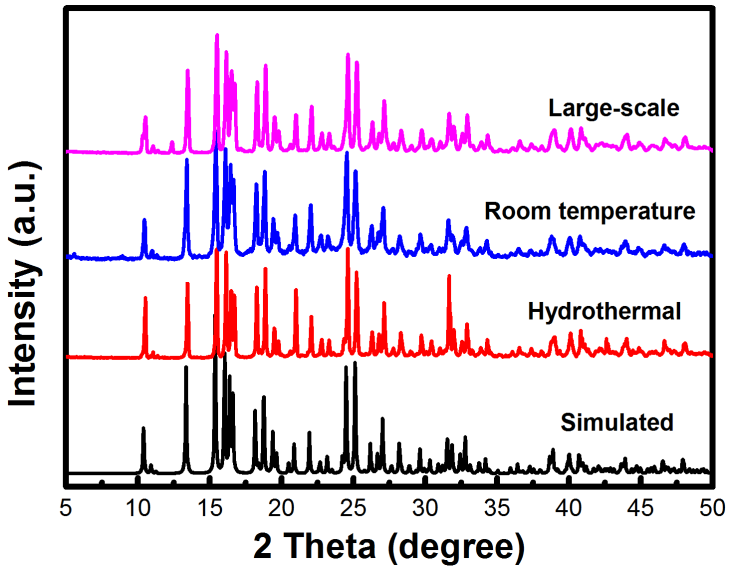

Figure S1. Powder X-ray diffraction (PXRD) patterns of synthesized $Zn_2(bpy)(btec)(H_2O)_2$ by different methods compared with simulated patterns.

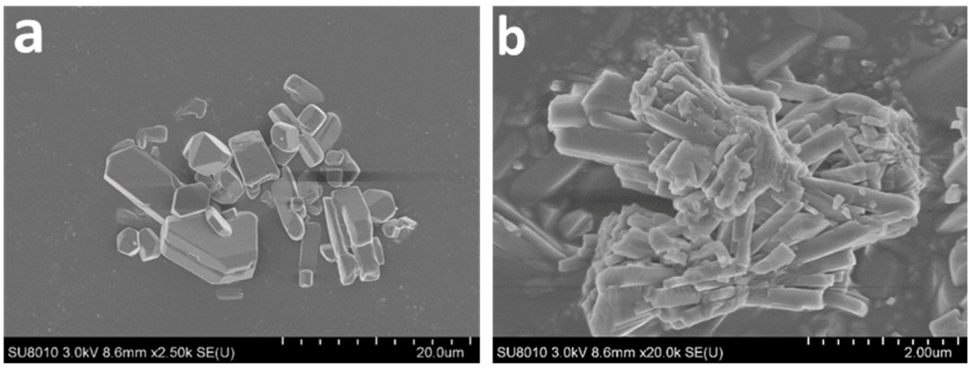

Figure S2. The SEM images of $[Zn_2(bpy)(btec)(H_2O)_2]\cdot 2H_2O$ synthesis by (a) hydrothermal synthesis and (b) room temperature synthesis.

4. Adsorption and pore characterization

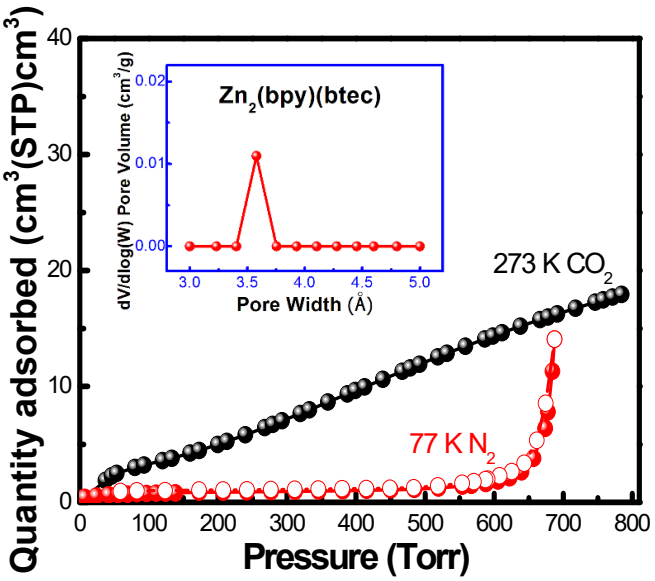

Figure S3. CO_2 sorption isotherms (273 K) and N_2 sorption isotherms (77 K) of Zn_2(bpy)(btec) by an ASAP 2020 Surface Area and Porosity Analyzer.

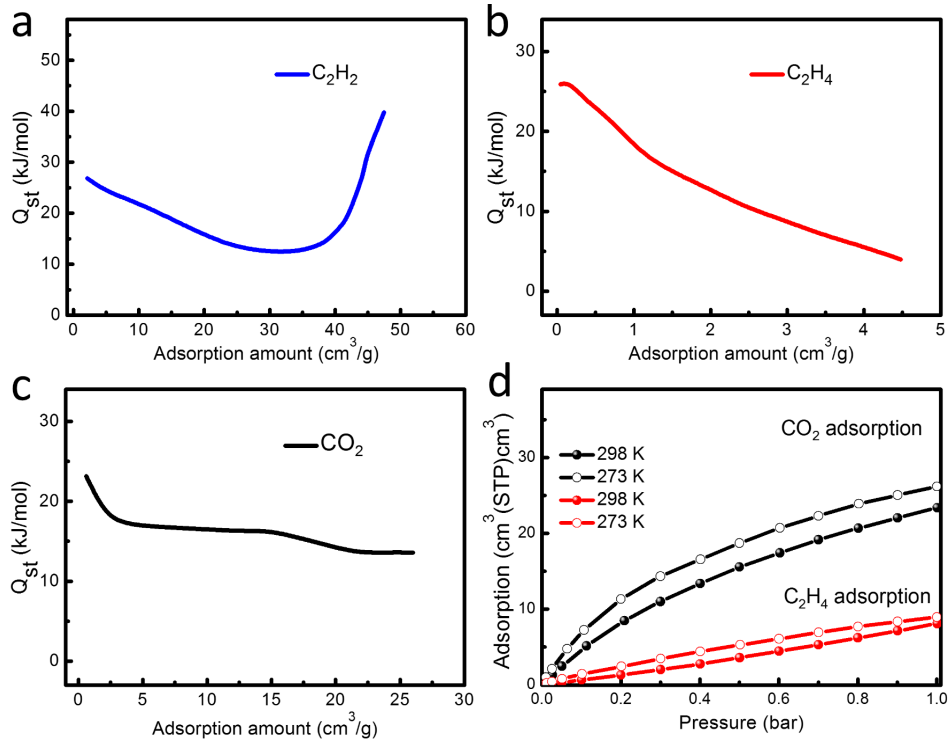

Figure S4. (a, b, c) Isosteric heats of C_2H_2, C_2H_4, and CO_2 adsorption in Zn_2(bpy)(btec) calculated by using the Clausius-Clapeyron equation. (d) C_2H_4 and CO_2 adsorption isotherms of Zn_2(bpy)(btec) at 273 K and 298 K.

5. Fitting of pure component isotherms

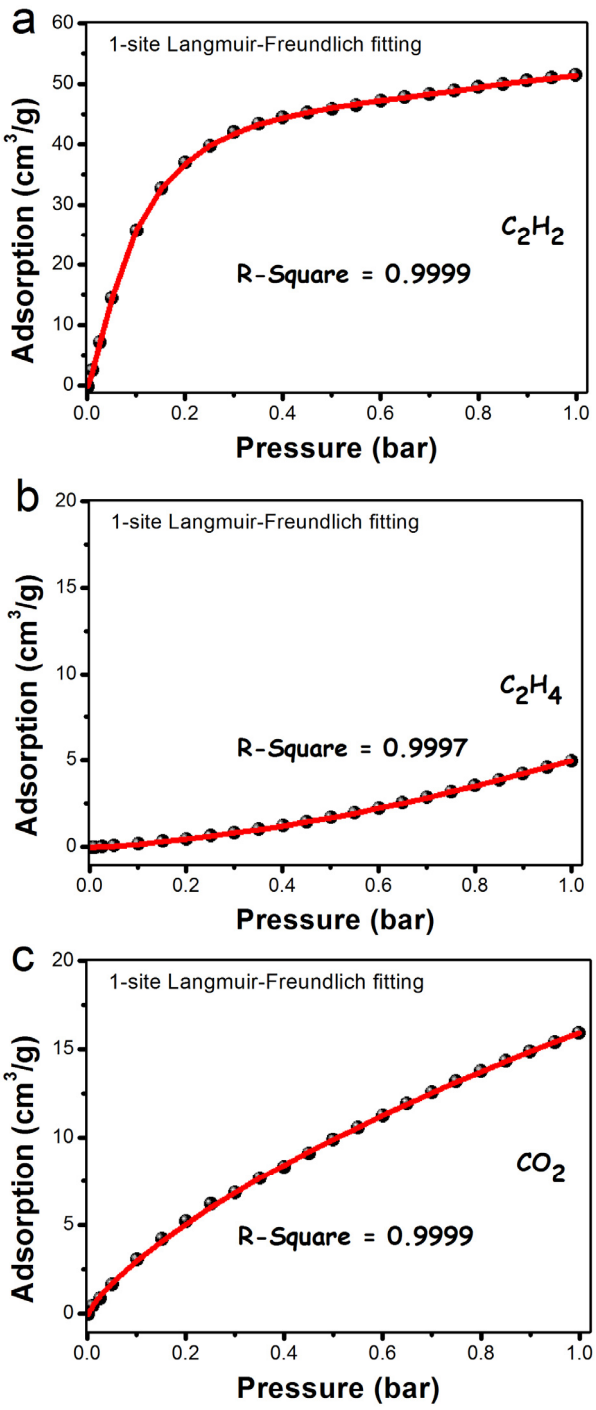

Figure S5. C_2H_2, C_2H_4 and CO_2 adsorption isotherms at 298 K in Zn_2(bpy)(btec) with the 1-site Langmuir-Freundlich model fits.

6. Breakthrough experiment and cyclic test

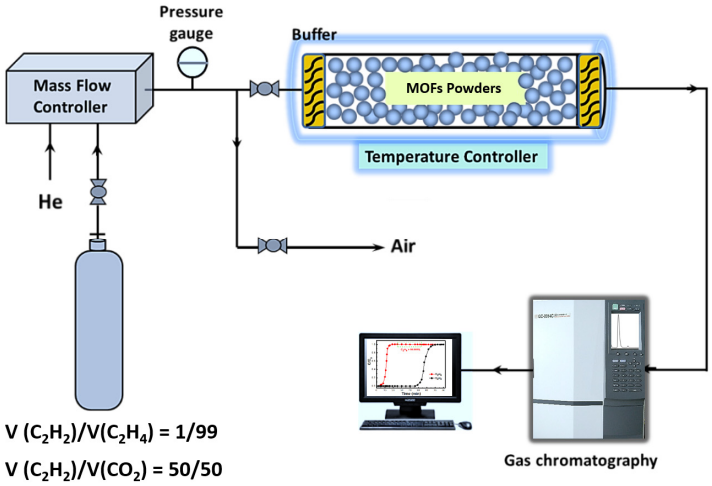

Figure S6. Breakthrough experiment apparatus.

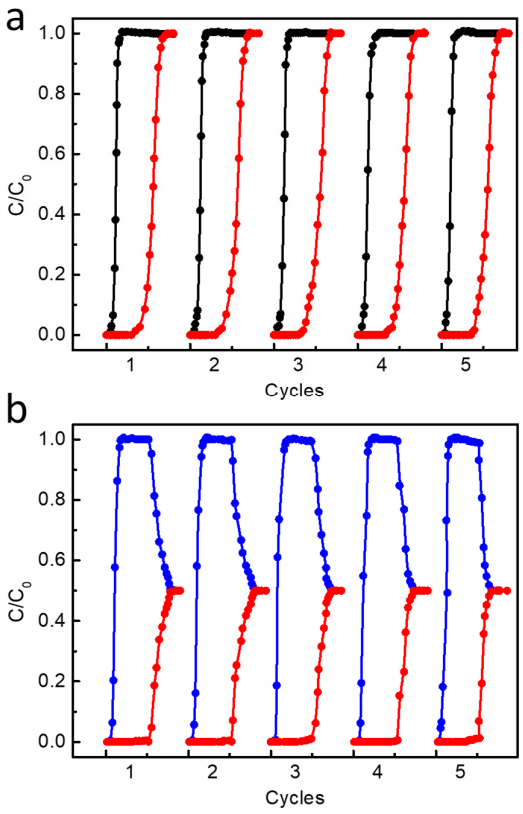

Figure S7. Cyclic breakthrough experiments for (a) C_2H_2/C_2H_4 (1/99, v/v) and (b) C_2H_2/CO_2 (50/50, v/v) on Zn_2(bpy)(btec) at 298 K and 1 bar, indicating Zn_2(bpy)(btec) maintained its separation performance at least 5 times.

7. Kinetic adsorption and desorption test

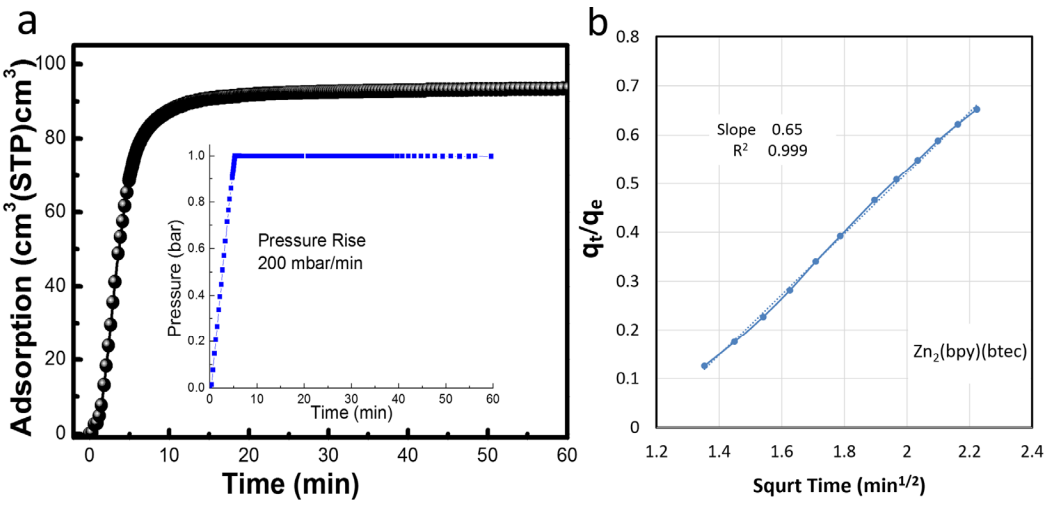

Figure S8. (a) Kinetic adsorption profiles for $Zn_2(bpy)(btec)$ at 298 K (Inset: diagram of pressure variation of C_2H_2). (b) Diffusional time constant calculation details of $Zn_2(bpy)(btec)$ for C_2H_2 adsorption at 298 K, the diffusion coefficient was estimated to 6.8×10^{-10} m^2/min based on the pressure increase rate of 200 mbar/min.

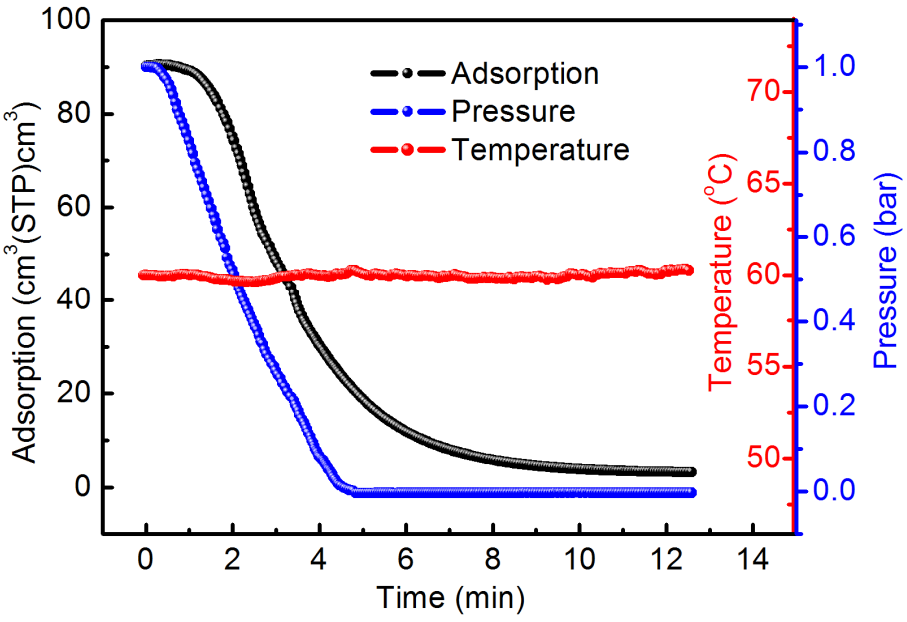

Figure S9. Kinetic desorption curves of C_2H_2 for $Zn_2(bpy)(btec)$ at 333 K with helium gas (50 mL/min).

8. Stability of C_2H_2 adsorption

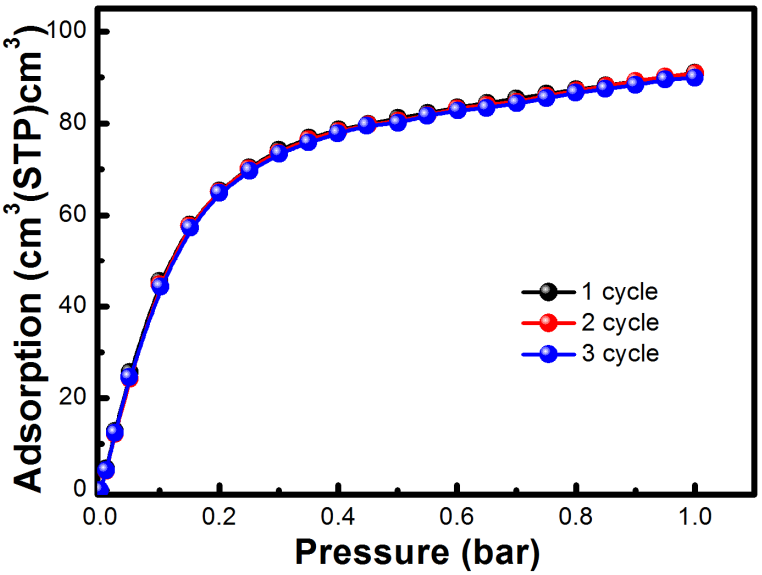

Figure S10. Cyclic C_2H_2 adsorption measurements on Zn_2(bpy)(btec) at 298 K and 1 bar, indicating that Zn_2(bpy)(btec) can maintain its C_2H_2 uptake capacity over three cycles.

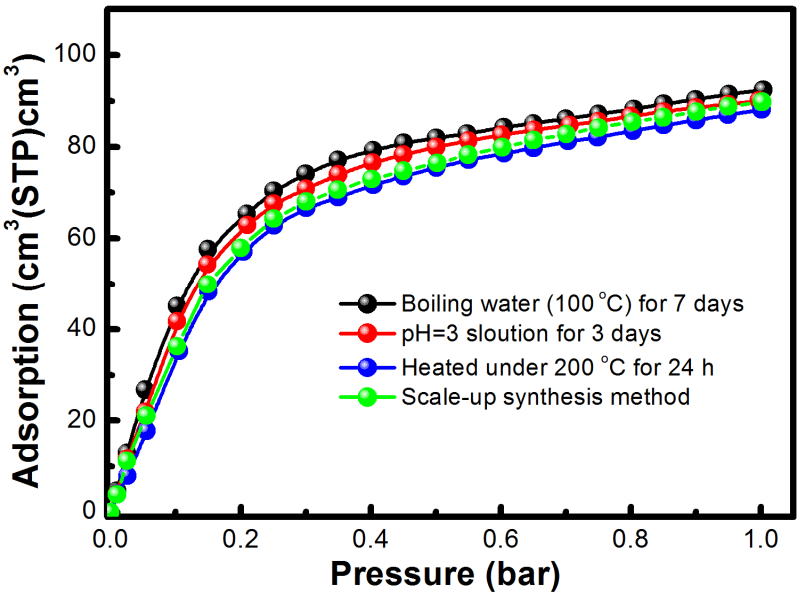

Figure S11. C_2H_2 adsorption isotherms for Zn_2(bpy)(btec) under different treatment at 298 K.

9. Structure chart and calculate parameters

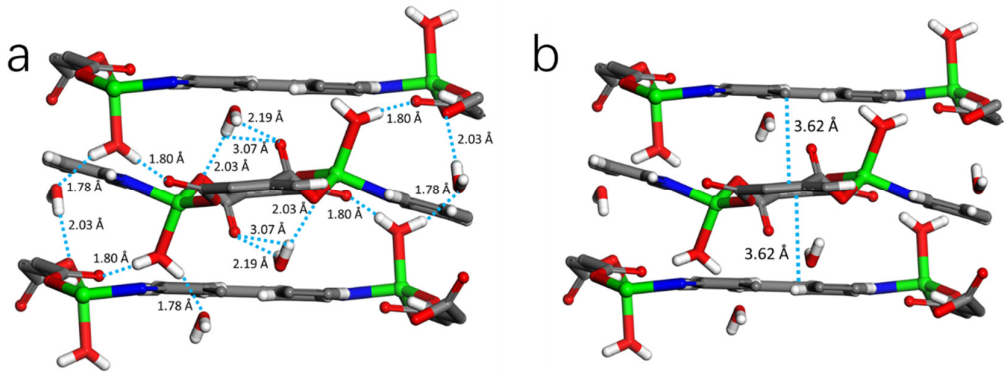

Figure S12. (a) Multiple hydrogen bondings and (b) offset π-π stacking interactions in the $[Zn_2(bpy)(btec)(H_2O)_2]\cdot 2H_2O$.

Table S1. Langmuir-Freundlich fit parameters for C_2H_4, C_2H_2, and CO_2 in $Zn_2(bpy)(btec)$.

	q_{sat} mol kg^{-1}	b_0 Pa^{-v}	v dimensionless
C_2H_2	2.55	8.403E-05	1
C_2H_4	1	1.028E-08	1.48
CO_2	1.6	7.812E-06	1

10. Comparison of parameters for various MOFs

Table S2. Summary of the adsorption uptakes, selectivity, heat of adsorption data and thermal stability in reported MOFs.

	Surface area (m^2/g, BET)	C_2H_2 uptake (mmol/g)	C_2H_4 uptake (mmol/g)	S_{ads}†	C_2H_2/C_2H_4 Uptake ratio※	Q_{st}§ (C_2H_2 kJ/mol)	Decomposition temperature (°C)	Ref.
UTSA-200a	612	3.65	0.63	6320	5.79	40	200	4
UTSA-100a	970	4.27*	1.66*	10.72	2.57	22	180	5
TIFSIX-2-Ni-i	480	4.21	2.42	22.7	1.74	40	272	6
SIFSIX-3-Zn	250	3.64	2.24	8.82	1.625	31	175	7, 8
SIFSIX-3-Ni	368	3.3	1.75	5.03	1.88	30.5	180	9
SIFSIX-2-Cu-i	503	4.02	2.19	44.54	1.84	41.9	219	6, 8
SIFSIX-2-Cu	1881	5.38	2.02	6	2.66	26.3	200	8, 10
SIFSIX-1-Cu	1178	8.5	4.11	10.63	2.07	37	160	8, 10
NOTT-300	1370	6.34‡	4.28‡	2.17	1.48	32	400	11
M'MOF-3a	110.1	1.9*	0.4*	24.03	4.75	25	380	12
Fe-MOF-74	1350	6.8#	6.1#	2.08	1.11	46	200	8, 13
ELM-12	706	2.56	1	14.8	2.56	25.4	320	14, 15
CPL-5	523&	3.01	1.84	6	1.6	31.3	214	16
CPL-2	495&	3.13	1.86	12	1.7	30.8	216	16
CPL-1	414&	2.07	0.31	26.8	6.7	40.2	218	16
NUC-2	1072	2.99	0.6	8.1	4.98	39.8	400	17
Zn_2(bpy)(btec)	**397&**	**2.3**	**0.223**	**107.8**	**10.31**	**28.7**	**410**	**this work**

Summary of the adsorption data were collected at 298 K

* At temperature of 296 K;

‡ At temperature of 293 K;

At temperature of 318 K;

† IAST selectivity for C_2H_2/C_2H_4 mixtures containing 1% C_2H_2 at 1 bar;

※ For ratios of the total uptake capacities at 1 bar;

§ Q_{st} values at low surface coverage;

& Surface area calculated from CO_2 isotherms.

Table S3. Summary of the adsorption uptakes, selectivity, heat of adsorption data and thermal stability in reported MOFs.

	Surface area (m^2/g, BET)	C_2H_2 uptake (mmol/g)	CO_2 uptake (mmol/g)	S_{ads}†	C_2H_2/CO_2 Uptake ratio※	Q_{st}§ (C_2H_2 kJ/mol)	Decomposition temperature (°C)	Ref.
HOF-3*	165&	2.1	0.94	21	2.24	20	350	18
UTSA-68*	897	3.13	1.78	3.4	1.77	26	280	19
UTSA-74	830	4.62	3.03	9	1.5	31	300	20
UTSA-83	70	0.53	0.17	6.2	3.1	24.4	150	21
UTSA-222a*	703	3.8	1.9	4	2	26	320	22
ZJUT-2*	350&	3.4	2.2	8.6	1.55	41.5	-	23
FJU-90a	1572	8.04	4.6	4.3	1.74	25.1	300	24
ZJU-195a	1722	9.55	4.68	4.7	2.04	29.9	260	25
TIFSIX-2-Ni-i	480	4.21	4.54	-	0.93	40	272	6
TIFSIX-2-Cu-i	685	4.1	4.3	6.5#	0.95	46.3	260	9
SIFSIX-3-Ni	223&	3.5	2.7	0.13#	1.3	36.7	210	9
FeNi-M'MOF	383	4.29	2.72	24	1.56	27	260	26
UPC-200(Fe)-F-H_2O	3192	5.39	2.4	2.25	2.25	19.9	350	27
UPC-200(Fe)-F-BIM	2213	6.24	2.4	2.94	2.6	20.5	350	27
Zn_2(bpy)(btec)	**397**	**2.3**	**0.71**	**33.3**	**3.23**	**28.7**	**410**	**this work**

Summary of the adsorption data were collected at 298 K

* At temperature of 296 K;

& Surface area calculated from CO_2 isotherms;

† IAST selectivity for C_2H_2/CO_2 (50:50, v/v) mixtures at 1 bar;

IAST selectivity for C_2H_2/CO_2 (2:1, v/v) mixtures at 1 bar;

※ For ratios of the total uptake capacities at 1 bar;

§ Q_{st} values at low surface coverage.

References

[1] R. B. Lin, L. Li, H. L. Zhou, H. Wu, C. He, S. Li, R. Krishna, J. Li, W. Zhou, B. Chen, *Nat. Mater.* **2018**, *18*, 1128-1133.

[2] S. S. Han, W. A. Goddard, *J. Am. Chem. Soc.* **2007**, *129*, 8422-8423.

[3] C. Zhang, L. Wang, G. Maurin, Q. Yang, *AIChE J.* **2018**, *64*, 4089-4096.

[4] B. Li, X. Cui, D. O'Nolan, H. M. Wen, M. Jiang, R. Krishna, H. Wu, R. B. Lin, Y. S. Chen, D. Yuan, H. Xing, W. Zhou, Q. Ren, G. Qian, M. J. Zaworotko, B. Chen, *Adv. Mater.* **2017**, *29*, 1704210.

[5] T. L. Hu, H. Wang, B. Li, R. Krishna, H. Wu, W. Zhou, Y. Zhao, Y. Han, X. Wang, W. Zhu, Z. Yao, S. Xiang, B. Chen, *Nat. Commun.* **2015**, *6*, 7328.

[6] M. Jiang, X. Cui, L. Yang, Q. Yang, Z. Zhang, Y. Yang, H. Xing, *Chem. Eng. J.* 2018, 352, 803-810.

[7] B. Desveaux, Adsorbed Gas Behaviour and Guest-Host Interactions in Ultramicroporous Metal-Organic Frameworks: *The University of Western Ontario*; 2017.

[8] X. Cui, K. Chen, H. Xing, Q. Yang, R. Krishna, Z. Bao, H. Wu, W. Zhou, X. Dong, Y. Han, B. li, Q. Ren, M. J. Zaworotko, B. chen, *Science* **2016**, *353*, 141-144.

[98] K.-J. Chen, Hayley S. Scott, David G. Madden, T. Pham, A. Kumar, A. Bajpai, M. Lusi, Katherine A. Forrest, B. Space, John J. Perry, Michael J. Zaworotko, *Chem* **2016**, *1*, 753-765.

[10] S. D. Burd, S. Ma, J. A. Perman, B. J. Sikora, R. Q. Snurr, P. K. Thallapally, J. Tian, L. Wojtas, M. J. Zaworotko, *J. Am. Chem. Soc.* **2012**, *134*, 3663-3666.

[11] S. Yang, J. Sun, A. J. Ramirez-Cuesta, S. K. Callear, W. I. David, D. P. Anderson, R. Newby, A. J. Blake, J. E. Parker, C. C. Tang, M. Schroder, *Nat. Chem.* **2012**, *4*, 887-894.

[12] S. C. Xiang, Z. Zhang, C. G. Zhao, K. Hong, X. Zhao, D. R. Ding, M. H. Xie, C. D. Wu, M. C. Das, R. Gill, K. M. Thomas, B. Chen, *Nat. Commun.* **2011**, *2*, 204.

[13] S. Bhattacharjee, J. S. Choi, S. T. Yang, S. B. Choi, J. Kim, W. S. Ahn, *J. Nanosci. Nanotechnol.* **2010**, *10*, 135-141.

[14] L. Li, R.-B. Lin, R. Krishna, X. Wang, B. Li, H. Wu, J. Li, W. Zhou, B. Chen, *J. Mater. Chem. A* **2017**, *5*, 18984-18988.

[15] Y. Zhang, P. Zhang, W. Yu, J. Zhang, J. Huang, J. Wang, M. Xu, Q. Deng, Z. Zeng, S. Deng,

ACS Appl. Mater. Interfaces **2019**, *11*, 10680-10688.

[16] F. Zheng, L. Guo, B. Gao, L. Li, Z. Zhang, Q. Yang, Y. Yang, B. Su, Q. Ren, Z. Bao, *ACS Appl. Mater. Interfaces* **2019**, *11*, 28197-28204.

[17] H. Chen, G. L. Zhuang, L. Fan, X. Zhang, L. N. Gao, D. Sun, *Chem. Commun.* **2020**, *56*, 2047-2050.

[18] P. Li, Y. He, Y. Zhao, L. Weng, H. Wang, R. Krishna, H. Wu, W. Zhou, M. O'Keeffe, Y. Han, B. Chen, *Angew. Chem. Int. Ed.* **2015**, *54*, 574-577.

[19] G. Chang, B. Li, H. Wang, T. Hu, Z. Bao, B. Chen, *Chem. Commun.* **2016**, *52*, 3494-3496.

[20] F. Luo, C. Yan, L. Dang, R. Krishna, W. Zhou, H. Wu, X. Dong, Y. Han, T. L. Hu, M. O'Keeffe, L. Wang, M. Luo, R. B. Lin, B. Chen, *J. Am. Chem. Soc.* **2016**, *138*, 5678-5684.

[21] H. Cui, S. Chen, H. Arman, Y. Ye, A. Alsalme, R.-B. Lin, B. Chen, *Inorg. Chim. Acta* **2019**, *495*, 118938

[22] J. X. Ma, J. Guo, H. Wang, B. Li, T. Yang, B. Chen, *Inorg. Chem.* **2017**, *56*, 7145-7150.

[23] H. M. Wen, C. Liao, L. Li, L. Yang, J. Wang, L. Huang, B. Li, B. Chen, J. Hu, *Chem. Commun.* **2019**, *55*, 11354-11357.

[24] Y. Ye, Z. Ma, R. B. Lin, R. Krishna, W. Zhou, Q. Lin, Z. Zhang, S. Xiang, B. Chen, *J. Am. Chem. Soc.* **2019**, *141*, 4130-4136.

[25] L. Zhang, K. Jiang, Y. Li, D. Zhao, Y. Yang, Y. Cui, B. Chen, G. Qian, *Cryst. Growth Des.* **2017**, *17*, 2319-2322.

[26] J. Gao, X. Qian, R. B. Lin, R. Krishna, H. Wu, W. Zhou, B. Chen, *Angew. Chem. Int. Ed.* **2020**, *59*, 4396-4400.

[27] W. Fan, S. Yuan, W. Wang, L. Feng, X. Liu, X. Zhang, X. Wang, Z. Kang, F. Dai, D. Yuan, D. Sun, H. C. Zhou, *J. Am. Chem. Soc.* **2020**, 142, 19, 8728–8737